Received: 17 July 2024 | Revised: 13 September 2024 | Accepted: 28 September 2024

DOI: 10.1002/bte2.20240025

RESEARCH ARTICLE

BATTERY ENERGY Open Access WILEY

Efficient and swift heating technique for crafting highly graphitized carbon and crystalline silicon (Si@GC) composite anodes for lithium-ion batteries

Chinmayee Padwal[1] | **Xijue Wang**[1] | **Hong Duc Pham**[2] | **Linh Thi My Hoang**[3] | **Sagadevan Mundree**[3] | **Deepak Dubal**[1]

[1]School of Chemistry and Physics, Centre for Materials Science, Queensland University of Technology, Brisbane, Queensland, Australia

[2]Centre for Future Materials, University of Southern Queensland, Toowoomba, Queensland, Australia

[3]School of Agriculture and Food Sustainability, The University of Queensland, Brisbane, Queensland, Australia

Correspondence
Deepak Dubal, School of Chemistry and Physics, Centre for Materials Science, Queensland University of Technology, Brisbane, QLD 4000, Australia.
Email: deepak.dubal@qut.edu.au

Abstract

The synthesis of battery materials from biomass as feedstock is not only effective but also aligns with sustainable practices. However, current methods like slow pyrolysis/heating are both energy-intensive and economically impractical. Hence, integrating energy-efficient technologies becomes imperative to curtail substantial energy consumption and, consequently, minimize carbon dioxide (CO_2) emissions during electricity usage. Herein, we employed a one-step pyrolysis/reduction based on the microwave heating method to synthesize a composite of high-purity silicon and highly graphitized carbon (Si@GC) from rice husk as feedstock. Compared to the conventional heating methods, the Si@GC samples prepared via the microwave heating method required less time (30–50 min). Benefiting from ultrahigh heating rates, the highly graphitized carbon and crystalline silicon composite was successfully synthesized. The synthesis by microwave irradiation showed homogenous material, excellent surface area, essential functional groups, and crystallinity revealing the outstanding reaction kinetics to form the material. The as-synthesized Si@GC composite anode material delivered a high discharge capacity of 799 mAh/g with high cyclic stability of ~71% over 120 cycles. The ex situ ToF-SIMS revealed great inorganic SEI composition, mainly consisting of the fluorinated species and carbonate species produced at the initial cycle. This investigation provides a novel rapid heating method for the synthesis of battery materials, which can also be extended for other materials and applications.

KEYWORDS

anode, lithium-ion battery, microwave irradiation, pyrolysis, rice husk

1 | INTRODUCTION

The increasing needs of the expanding population have presented in two major global challenges, namely the energy crisis and solid waste management, which results in notable environmental consequences. It is imperative for a circular economy to address sustainable development objectives and formulate approaches for transforming agricultural and biowaste into energy through the application of advanced technological processing methods, thus tackling these significant challenges. First, energy-saving technology should be utilized to reduce the use of extensive energy, thereby reducing CO_2 emission during electricity generation. Second, agro-biomass accumulation on land should be mitigated by making better use and eradicating combustion, which limits the emission of harmful gases in the environment. Currently, the conversion process of biomass to useful materials involves long-hour pyrolysis under an inert or air atmosphere in the conventional furnace or hydrothermal carbonization.[1–3] The conventional furnace allows the slow conversion carbonization involving a minimum of 5 h to obtain the nanocomposite material. This system has been actively utilized in solid waste management, waste minimization, and product development in major industries. This process is not only lengthy to obtain good-quality products but also consumes a lot of electricity.

Pyrolysis (heating) processes are typically categorized based on the rate at which the biomass particle is heated to the pyrolysis temperature. Consequently, a distinction can be drawn between fast and slow pyrolysis. Fast pyrolysis/heating is characterized by operating conditions that aim to optimize the production of the active material, such as high heating rates and short vapor residence times. The resulting pyrolyzed material is considered a raw liquid biofuel that can be utilized in stationary heat and power applications or, alternatively, can undergo further refinement for use as a drop-in transportation biofuel. The majority of research efforts in the field of biomass pyrolysis have focused on fast pyrolysis.[3,4] Recently, some preliminary investigation has been conducted on the process of pyrolysis driven by microwaves. The utilization of microwaves for heating differs fundamentally from all other pyrolysis methods because the biomass is heated internally rather than through external heat transfer from a heat source of elevated temperature. Microwave heating (MWH) is an electromagnetic heating method that employs microwave radiation to transfer energy to the materials undergoing heating. In contrast to conventional heating techniques that utilize a surface-to-inside mechanism, microwave heating operates through a direct, uniform, and instantaneous inside-to-surface heating mechanism explained in Figure 1. Consequently, microwave irradiation proves highly advantageous since it ensures uniform molecular-level heating followed by rapid heating of the entire volume. MWH offers several advantages, including a rapid, uncomplicated, and cost-effective process, as well as the production of high-quality and high-yield products. MWH results in an escalation of the carbon yield, an enhancement in the quality of material, a provision of elevated energy efficiency, and a reduction in the formations and emissions of perilous substances, thus ultimately rendering the method ecologically sound. Nonetheless, despite these benefits, microwave synthesis encounters certain challenges that necessitate further research to optimize the process.[5–7]

RH-derived silicon/carbon anode materials are widely recognized as the most popular and efficient anode material for lithium-ion batteries due to their exceptional electrical conductivity and structural integrity. However, the primary obstacle lies in the pyrolysis process, which has been discussed previously. Recently, Wang et al.[8] made a notable advancement by employing rapid direct heating at an ultrahigh rate to synthesize high-purity LNMO crystals in a mere 2 h instead of the conventional 15 h. This improvement is significant in comparison to traditional methods. Additionally, microwave irradiation has been found to enhance reaction kinetics and improve the homogeneity of LNMO, as reported by Wang et al.[8] Furthermore, Praneetha and Murugan[9] have reported a process that involves microwave-assisted solid-state ashing followed by a magnesiothermic reaction to convert silicon using RH. In most cases, a carbon coating is applied to silicon nanomaterial as a common practice.[10–13] However, this intricate process demands a considerable amount of energy as it entails a two-step conversion involving pyrolysis and heating. Consequently, research indicates a substantial gap in the utilization of energy-efficient techniques such as microwave irradiation for biomass conversion during the pyrolysis process.

In the present investigation, we have demonstrated the effective ultra-fast pyrolysis/reduction method to produce crystalline silicon and highly graphitized carbon (Si@GC). Furthermore, the microwave pyrolysis/reduction process was optimized at distinct temperatures and times to achieve optimal battery performance as anode material for LIB. The resulting material exhibited an exceptional quality, characterized by partially carbonized crystalline carbon and silicon, which in turn showcased remarkable properties. The solid electrolyte interface (SEI) formation mechanism

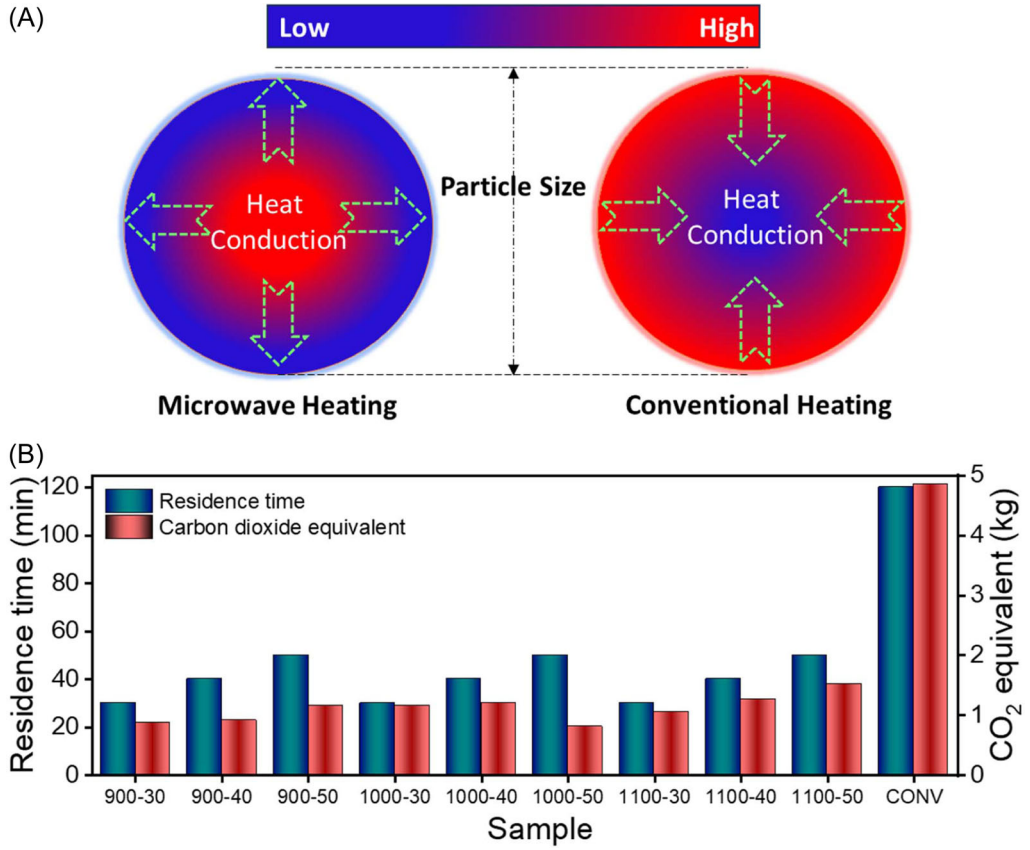

FIGURE 1 (A) Schematic illustration of particle heating mechanism in conventional and microwave pyrolysis process at 900, 1000, and 1100 for residence time of 30, 40, and 50 min, (B) residence time and CO_2 equivalent (kg) of microwave and conventionally heated samples.

and composition were uncovered using advanced time-of-flight secondary ion mass spectrometry (ToF-SIMS).

2 | EXPERIMENTAL DETAILS

2.1 | Synthesis of silica/carbon nanocomposite

Rice husks, kindly provided by SunRice food company, underwent a pretreatment process at a temperature of 100°C for 4 h. This pretreatment involved the use of a deep eutectic solvent, specifically choline chloride and oxalic acid in a ratio of 1:2 (ChCl:OA), to eliminate any organic and metal impurities present in the husk. Following this, the pretreated rice husk samples were filtered, washed with deionized water, and subsequently dried at a temperature of 80°C overnight. As a result, the dried samples were then subjected to cryo-milling for 1 min at 30 Hz frequency with a mixture of magnesium and sodium chloride, with a ratio of 1:0.7:1 for rice husk, magnesium, and sodium chloride, respectively.[14] These mixtures were then pyrolyzed under inert conditions at three different temperatures, specifically 900°C, 1000°C, and 1100°C, with varied holding periods of 30, 40, and 50 min using microwave irradiation furnace. The samples were washed to remove the metal residue using 1M HCl, distilled water, and ethanol. This pyrolysis process aimed to synthesize the desired silicon/carbon composites through carbonization. The resulting materials were denoted as MW-900-30, MW-900-40, MW-900-50, MW-1000-30, MW-1000-40, MW-1000-50, MW-1100-30, MW-1100-40, and MW-1100-50, respectively. To eliminate any remaining impurities, the synthesized material was washed with a 1M solution of hydrochloric acid and subsequently dried in a vacuum oven at a temperature of 70°C overnight.

2.2 | Material characterizations

The composition of the surface was determined through the utilization of X-ray photoelectron spectroscopy (XPS) measurements employing a Kratos AXIS Supra spectrometer. To examine the morphology of materials at the surface, field emission scanning electron microscopy (FE-SEM) using a Tescan-MIRA3 instrument, transmission electron microscopy (TEM), and high-resolution TEM (HR-TEM) with a

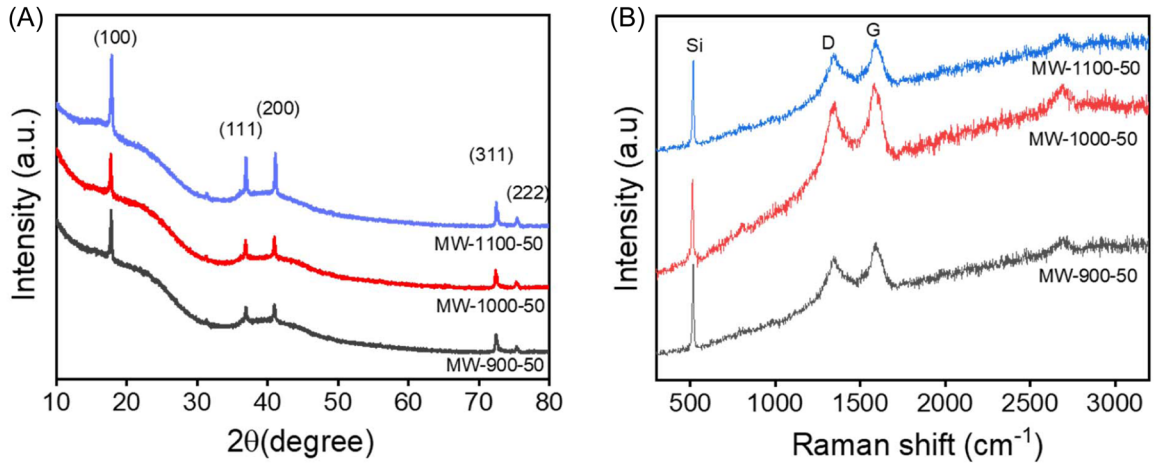

FIGURE 2 (A) XRD, and (B) Raman spectra of MW-900-50, MW-1000-50, MW-1000-50 obtained by microwave heating process.

JEOL 2100–200 kV instrument were employed. For the determination of the surface area, N_2 adsorption-desorption experiments were conducted using Micromeritics 3 Flex. The Raman microscope Renishaw was employed to acquire Raman spectra of the material, utilizing a selective laser source at a 532 nm wavelength.

2.3 | Electrochemical characterization

The electrochemical evaluation of MW-900-30, MW-900-40, MW-900-50, MW-1000-30, MW-1000-40, MW-1000-50, MW-1100-30, MW-1100-40, and MW-1100-50 samples as anode materials in lithium-ion batteries (LIBs) was executed utilizing CR2032 coin-type half-cells, assembled in a argon-filled glovebox. The formulation of the electrode was obtained through the blending of the active materials, super P, and poly (vinylidene fluoride) (PVDF) binders in an 80:10:10 weight ratio, followed by the creation of a paste employing an N-methyl-2-pyrrolidone (NMP) solution. Subsequently, the paste was administered onto copper foil and dried in a vacuum oven at 80°C for a duration of 12 h. The cell configuration encompassed lithium metal as the counter electrodes, glass microfiber separator, and SC derivatives. The mass loading varied from 0.5 to 0.73 mg across a diameter 12 mm electrode. The electrochemical evaluation of the material was carried out employing commercially available 1M lithium hexafluorophosphate (LiPF6) dissolved in ethylene carbonate (EC)/diethyl carbonate (DEC)/dimethyl carbonate (DMC) with a volume ratio of 1:1:1 (Sigma). The cells underwent cycling within the range of 0.01 to 3.0V (vs. Li/Li+). The galvanostatic charge/discharge (GCD) tests were executed by utilizing Neware battery testers, while cyclic voltammetry data were acquired using a Biologic VMP-300 potentiostat. Furthermore, ex situ Raman, X-ray photoelectron spectroscopy (XPS), scanning electron microscopy (SEM), and time-of-flight secondary ion mass spectrometry (ToF-SIMS) analysis were performed.

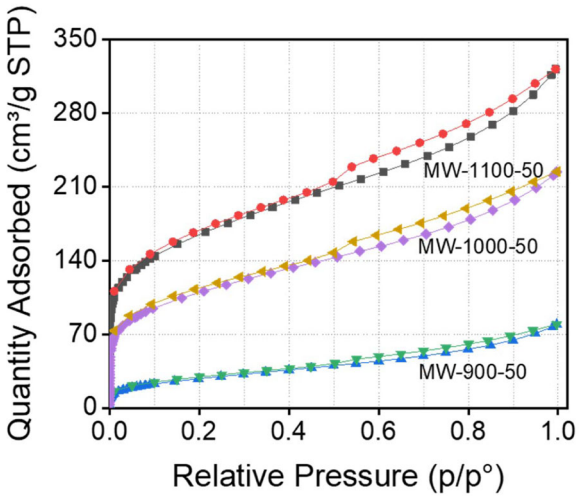

FIGURE 3 BET of the samples, MW-900-50, MW-1000-50, and MW-1100-50 obtained by microwave heating process.

3 | RESULTS AND DISCUSSION

3.1 | Determination of CO_2 emissions

Most of the processes involved in converting biomass into materials are characterized by high energy consumption, starting from the initial biomass drying stage to the subsequent pyrolysis process. The utilization of energy-intensive methods gives rise to significant emissions of CO_2 and other greenhouse gases

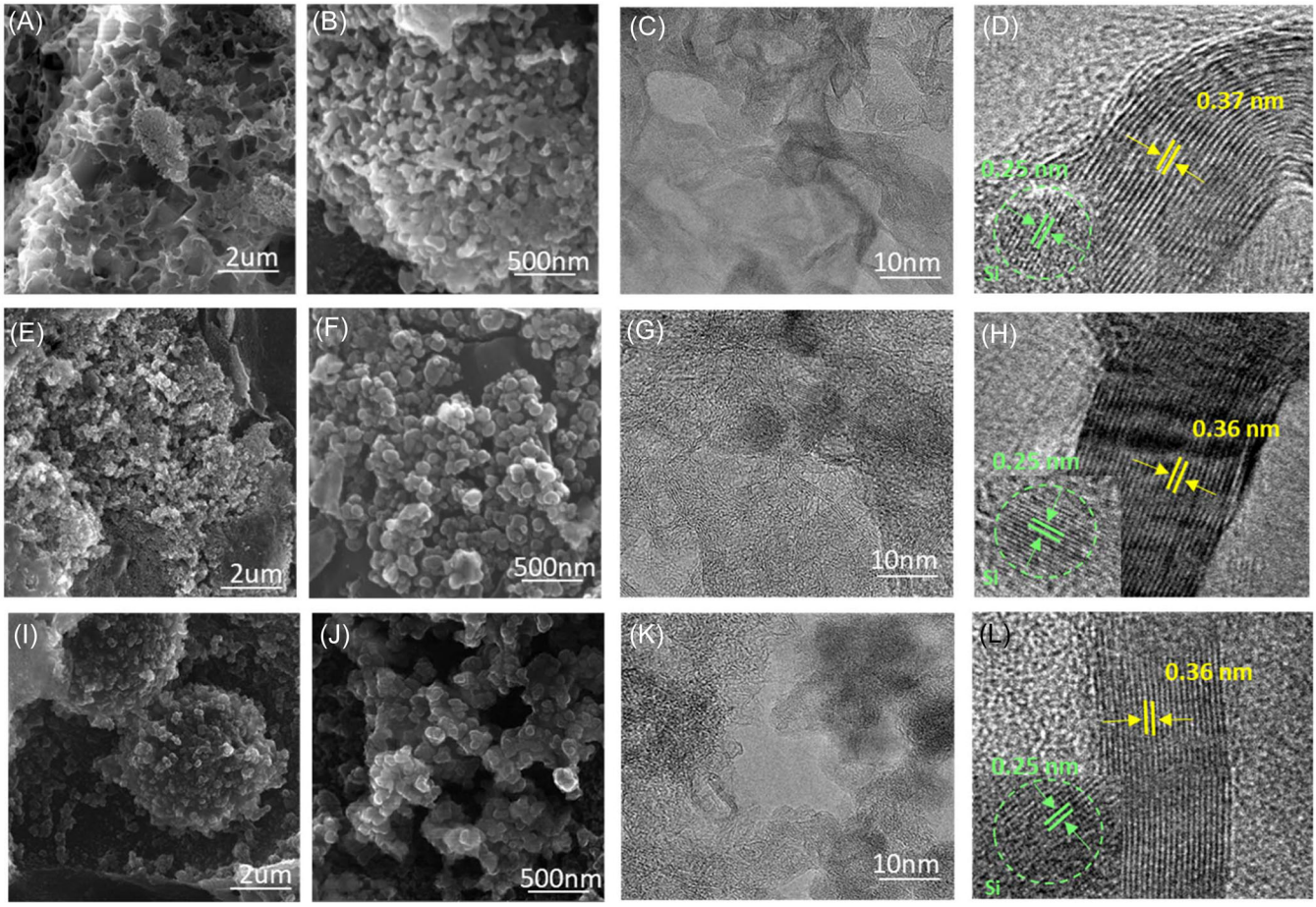

FIGURE 4 FE-SEM and HR-TEM analysis of the samples, (A–D) MW-1100-50, (E–H) MW-1000-50, and (I–L) MW-900-50 obtained by microwave heating process.

(GHG). Therefore, it is crucial to conduct a thorough analysis of the energy requirements for both the primary process and any subsequent postprocessing stages to determine the most energy-efficient and environmentally friendly approach. In this study, the impact of using conventional and microwave methods to produce biomass-derived anode materials on residence time and CO_2 emissions was examined and depicted in Figure 1B.

The quantities of CO_2 are determined by evaluating the electricity consumption and emission factor as indicated in Figure 1A. The use of the microwave furnace for the synthesis of Si@GC composite has markedly diminished CO_2 discharge when compared to the conventional procedure. The primary rationale behind this is the accelerated heating rate and abbreviated duration of exposure to heat in the microwave method. In greater detail, the time required to raise the temperature of the samples from room temperature to 900°C, 1000°C, and 1100°C in the microwave furnace was less than 90 min, which is approximately 1.7 times faster than the conventional method. The dissimilarity in heating efficiency can be ascribed to the unique mechanism of microwave heating, which directly heats the substance through molecular dipole rotation and friction. Consequently, a more efficient and uniform heating of the material occurs, resulting in an improved heating speed and decreased thermal gradients. Furthermore, the sharp thermal gradient observed in the microwave heating curve may also contribute to a notable reduction in CO_2 discharge in comparison to the conventional heating technique. This effect is due to the swifter heating speed and enhanced heating efficiency of microwave heating, and it has the potential to considerably diminish energy consumption and greenhouse gas emissions during the manufacturing and processing of materials.

3.2 | Analysis of Si@GC materials

The structural characteristics of the samples were investigated using the XRD technique. Although there is a slight shift in the peaks, all the samples in Figures 2A and S6a,c show the presence of crystalline carbon and

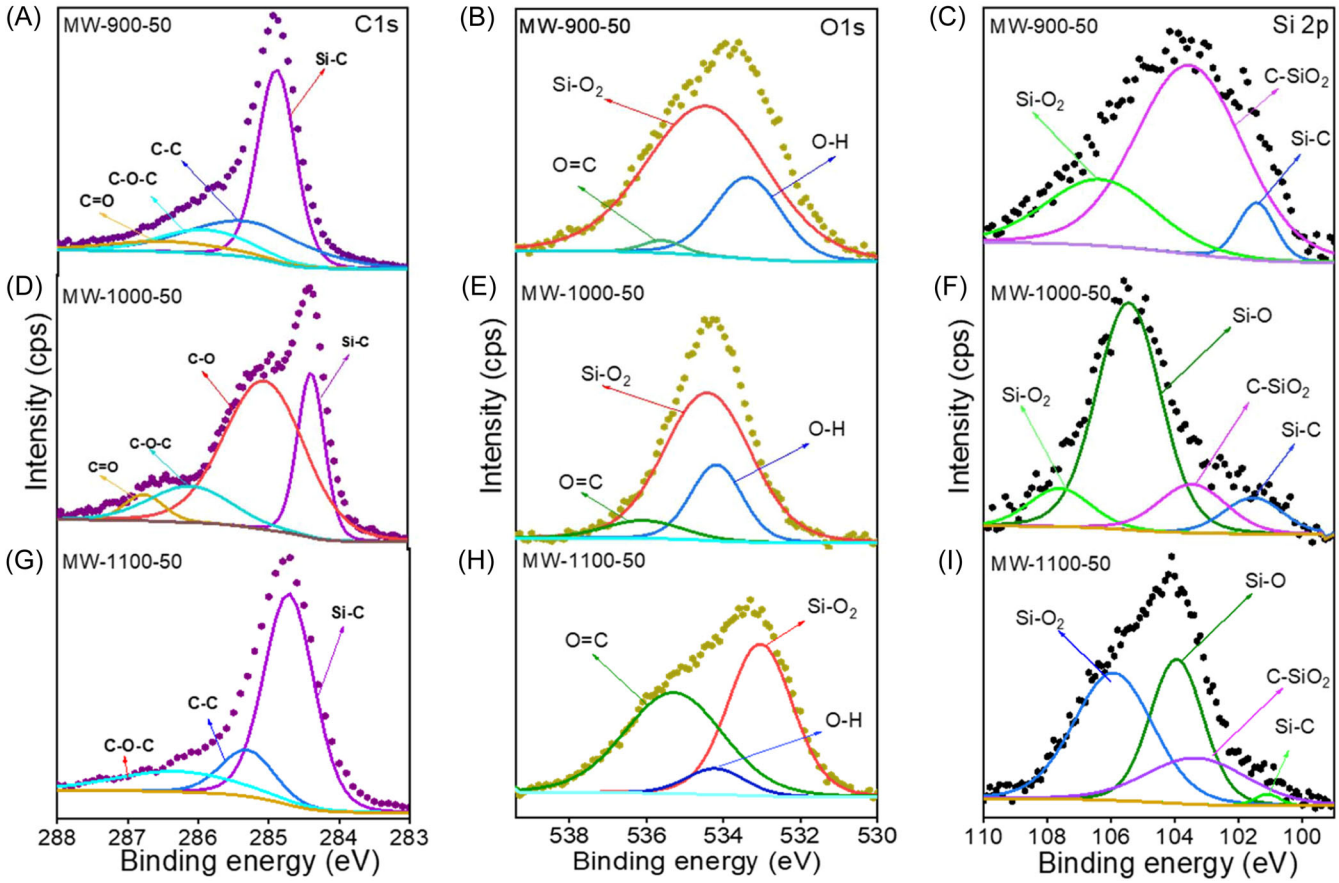

FIGURE 5 The XPS data consisting of functional groups including C1s, O1s, and Si2p for (A–C) MW-900-50, (G–I) MW-1100-50, and (D–F) MW-1000-50 samples.

silicon, as well as a peak for silicon carbide. The peak at approximately ~18° corresponds to the (100) plane of graphitic carbon structures. The crystalline β-SiC strong bond at the lattice peak observed at around ~36.7° and ~40.9° corresponds to (111) and (200) plane, followed by a pure silicon peak at approximately ~72° and ~75° correlating to the reflection of the plane (311) and (222). XRD analysis also reveals the presence of an amorphous phase of silica and carbon. The quality of the material under microwave irradiation heating remains unaffected and actually improves with longer holding time.[15]

Raman spectra is depicted in Figure 2B. All the samples exhibit a noticeable peak at approximately 510 cm^{-1}, which is attributed to the pure silicon. Moreover, the two other peaks observed at 1346 cm^{-1} and 1583 cm^{-1} are identified as the D-band originating from disordered carbon and the G-band arising from sp2 graphitic carbon, respectively. In terms of qualitative assessment, the Raman spectrum enables the observation of the level of amorphousness and the presence or absence of defects in carbon materials. To quantitatively evaluate this, the ratio of the G band to the D band can be analyzed to obtain degree of amorphousness data. Specifically, a higher degree of graphitic crystallinity corresponds to a lower intensity ratio and a reduced number of defects. The ID/IG ratio of ~0.85 displays crystalline carbon, indicating the presence of certain defects or a certain degree of amorphous characteristics in the carbon material derived from RH. The intensity of graphitization is observed to decrease in the case of a shorter holding time during microwave irradiation, as shown in Figure S6b,d, thus impacting the quality of the carbon structure.[16] This is in concurrence with the findings on surface area. The adsorption-desorption isotherms obtained via Brunauer–Emmett–Teller (BET) analysis (Figure 3, ESI†) indicate that the specific surface areas for samples obtained at 50 min at 900°C, 1000°C, and 1100°C are calculated to be 11.51, 381.74, and 571.22, respectively. The increase in temperature has a significant impact on the surface area of the silicon carbon nanocomposite. Table S1 and Figure S7 present the BET values of all samples obtained at 30 and 40 min at the selected temperature. The BET values of the Si@GC composite samples converted from biomass suggest that higher temperatures result in superior porosity and surface area compared to those obtained at lower temperatures with microwave irradiation.

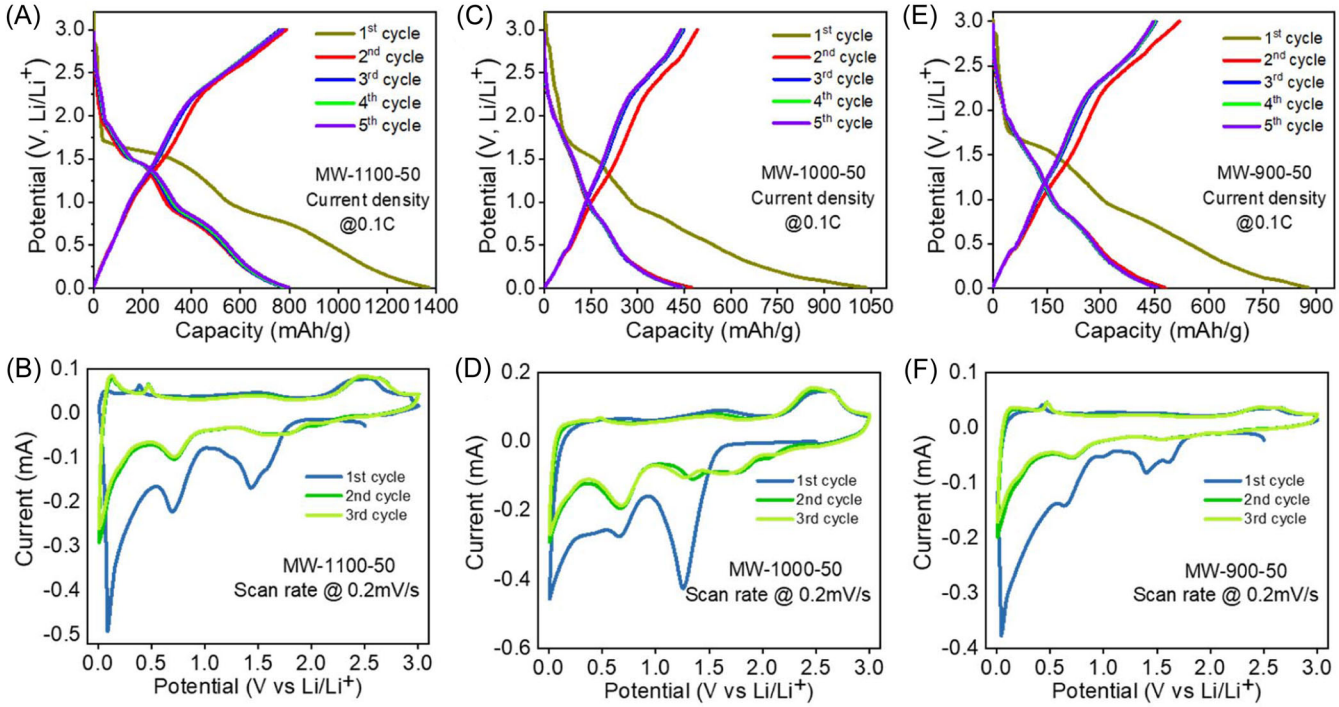

FIGURE 6 GCD and CV electrochemical measurements for (A and B) MW-1100-50, (C and D) MW-1000-50, and (E and F) MW-900-50 anode materials.

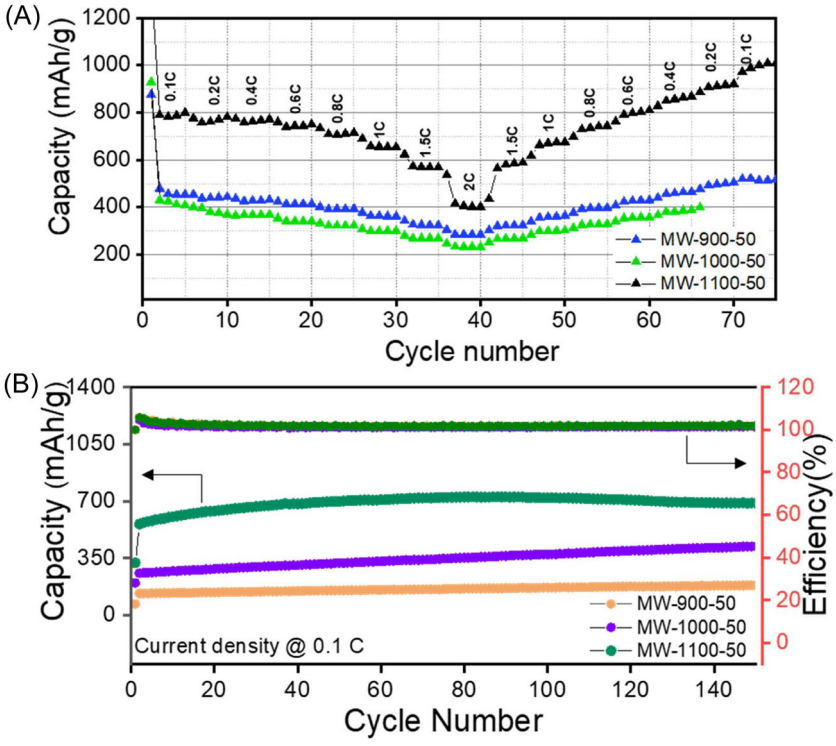

FIGURE 7 (A) Rate performance and (B) cyclic stability for MW-1100-50, MW-1000-50, and MW-900-50 obtained by microwave heating process.

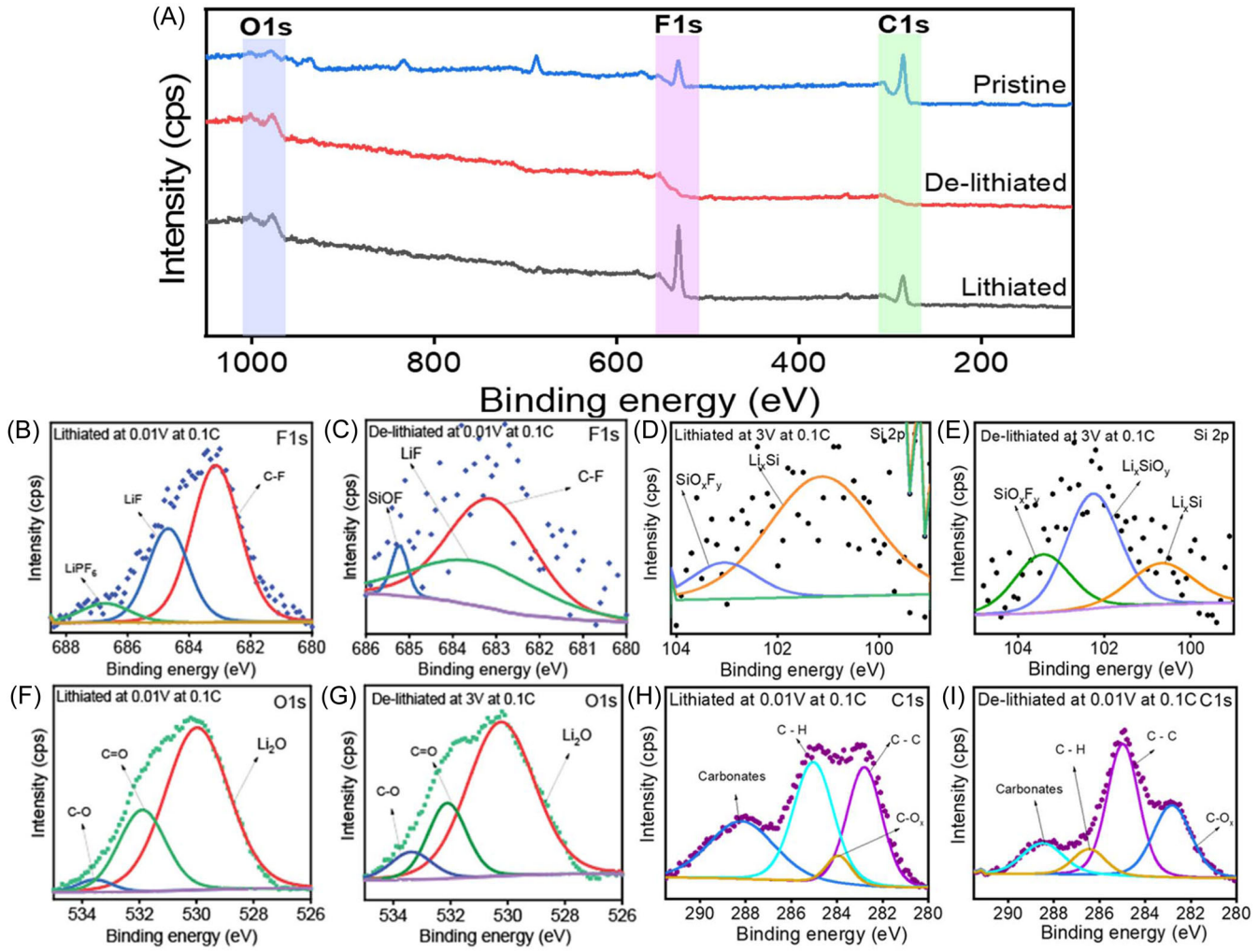

FIGURE 8 Ex situ XPS analysis of MW-1100-50 electrode lithiated and delithiated in $LiPF_6$ for LIB at 0.1C current density, high resolution spectra for lithiated electrode (A) wide spectra, (B) F1s, (D) Si2p, (F) O1s, (H) C1s, and (C) high resolution spectra for delithiated electrode (C), F1s, (E) Si2p, (G) O1s, (I) C1s.

Figures 4, S1, and S2 depict the surface morphology of the samples, which was recorded using SEM and TEM. The SEM images disclose the presence of conglomerates of spherical Silicon (Si) nanocrystals within the samples. These nanocrystals are interconnected, leading to the formation of densely aggregated nanoparticles that are evenly dispersed across the surface of the carbon material. The HRTEM images (Figures 4, S1, and S2) reveal the interfaces between Silicon Carbide (SiC) and carbon. The presence of distinct lattice fringes, with an interlayer spacing of 0.25 nm, corresponds to the (111) crystal plane of cubic β-SiC. Moreover, besides the SiC, there are also carbon domains that can be identified with an interlayer distance of 0.34 nm (Figures 4, S2, and S6a-c) indicating the partially graphitized nature of the carbon.[17,18] It is observed that when treatment temperatures increase, graphitization occurs. HR-TEM studies confirm that longer treatment times and temperatures above 1000°C cause ordering of disordered carbons and ultimately lead to stable graphitization. This process evolves over time and occurs at various temperatures. Initially, amorphous carbon forms a lamellar network with graphitic bonding. Small clusters of six-membered rings create networks similar to the carbonization process described by Patrick.[19] Furthermore, the confirmation of the formation of the nanocomposite structure can also be established based on its distinctive Raman scattering properties.

Furthermore, XPS analysis was used to investigate the surface composition and chemical states of elements in the Si@GC composite samples. Figure 4 displays the high-resolution Si 2p (Figure 5C,F,I, C 1s Figure 5A,D,G, and O 1s Figure 5B,E,H) spectra for all samples. The Si 2p region reveals peaks and is assigned to 101(Si-C), 103 (C-SiO_2), 104 (SiO), and 106 (SiO_2) in all the samples at carbonized for 50 min at 1100°C, 1000°C, and 900°C. The C 1s spectrum is deconvoluted into main peaks for all samples, Si-C (~284 eV), C-C (~285 eV), C-O-C (286.8 eV), and C=O

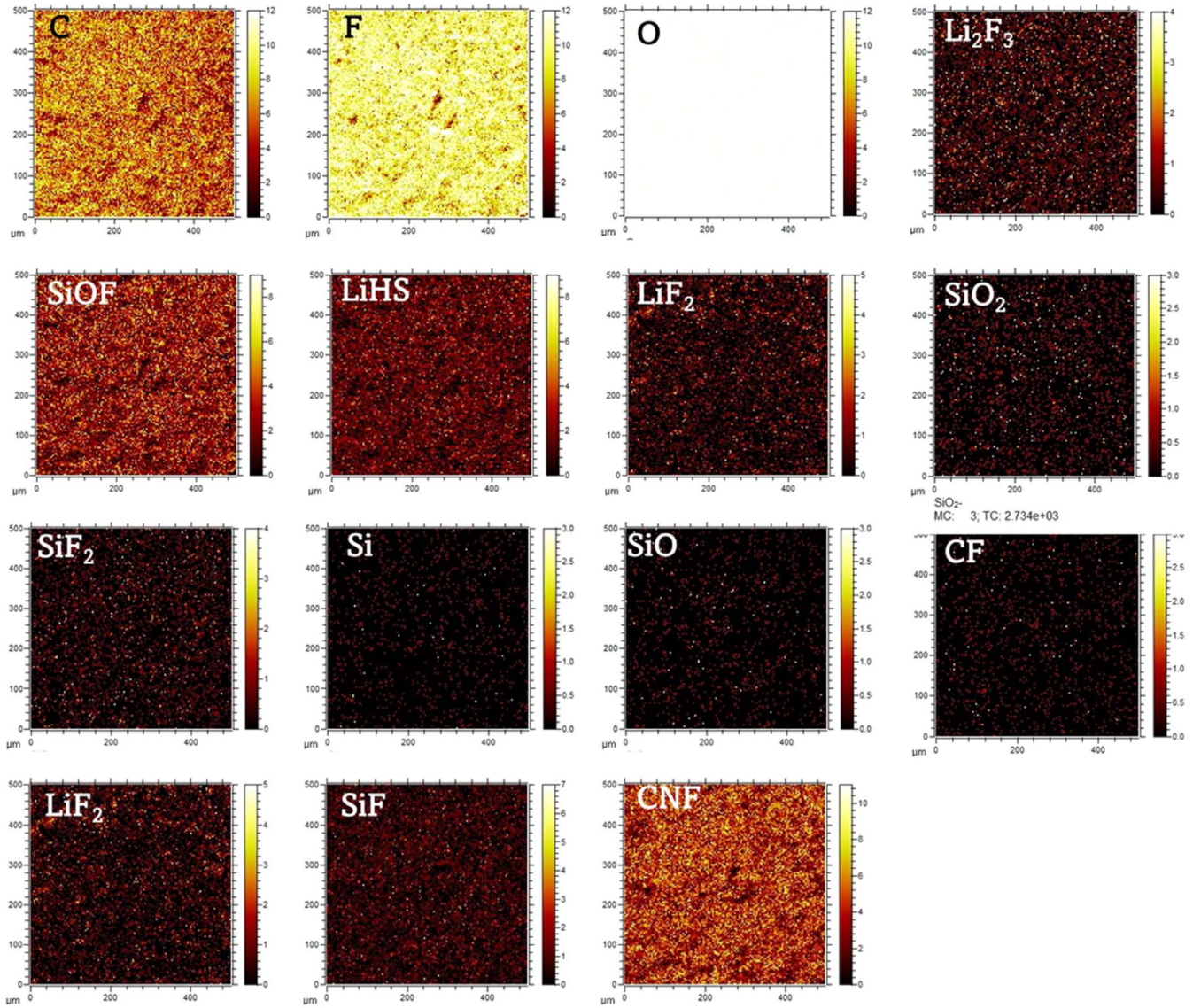

FIGURE 9 ToF-SIMS imaging analysis in negative ion mode of MW-1100-50 electrode lithiated in $LiPF_6$ for LIB at 0.1C current density at 0.01 V.

(286.6 eV). However, at MW-1100-50, the C=O group is seen missing. Furthermore, the high-resolution O 1 s spectra depicts the chemical bonding state of O, with peaks corresponding to C=O (~535.4 eV), Si-O2 (~535 eV), and O-H (~534.4 eV) seen in all samples obtained at 50 min of microwave irradiation. Similarly, Figures S3–S5 show the XPS plots for 30 and 40 min for the Si 2p, C 1s, and O 1s spectra.

3.3 | Electrochemical measurements

The electrochemical behavior of MW-900-50, MW-1000, and MW-1100 at 30′, 40′, and 50'min Si@GC composite obtained using microwave irradiation are further assessed in lithium-ion half-cells as an anode material. The cyclic voltammetry (CV) and galvanostatic charge/discharge (GCD) examinations are conducted within the range of 0.01–3.0 V (vs. Li metal counter electrode). The CV profiles of these silicon/carbon anodes at 0.2 mV/s for the initial three cycles are depicted in Figures 6B,D,F, S8b,d,f, and S9b,d,f encompassing all the samples. Generally, the lithiation and delithiation peaks at potentials typical of the reaction of anodic Si are evident in all samples. During the initial cathodic half-cycle (lithium uptake), distinct peaks are observed at 0.2 and 2.5V corresponding to the intercalation of the Li-ions. Furthermore, cathodic peaks emerge at ~0.6V in the first CV cycle and are associated with the development of solid electrolyte interphase (SEI) and the degradation of the electrolyte.[20] Subsequently, these peaks vanish in the following cycles, indicating the presence of a stable SEI layer and the reversible performance of the electrodes. The cathodic peak

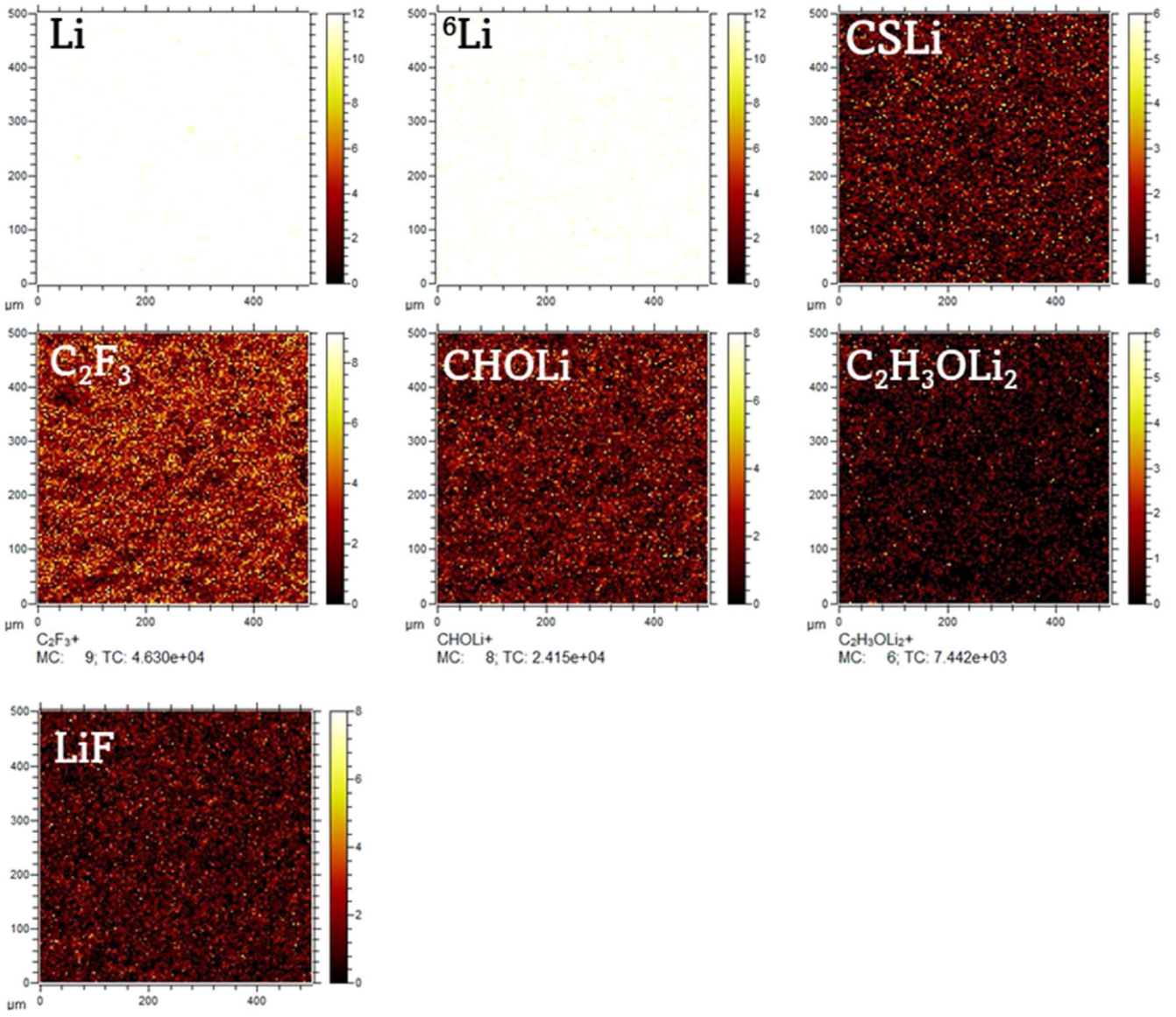

FIGURE 10 ToF-SIMS imaging analysis in positive ion mode of MW-1100-50 electrode lithiated in $LiPF_6$ for LIB at 0.1C current density 0.01V.

appearing at 1.6 V is linked to the creation of LixC and LixSi alloy phases and is consistent across all the samples.[21,22] Additionally, when compared to the initial scan, the magnitude of the anodic current peaks in the second and third scans exhibits a slight expansion, likely due to the gradual disintegration of the crystalline silicon structure as lithium ions infiltrate the silicon host and form the amorphous Li-Si alloy.[23]

The galvanostatic charge-discharge (GCD) curves of all the samples are displayed in Figures 6A,C,E, S8a,c,e, and S9a,c,e. The first five cycles of all the samples at the current density of 0.1C and full delithiation process of anode samples MW-900-50, MW-1000-50, and MW-1100-50 delivered the initial reversible discharge capacities of 476, 429, and 799 mAh/g. The initial coulombic efficiency of 58%, 59%, and 47% was estimated for all the samples, respectively. Furthermore, the initial capacity for the sample MW-900-30, MW-1000-30, and MW-1100-30 was 309, 534, and 300 mAh/g, with initial Coulombic efficiency of 32%, 43%, and 49%. Subsequently, the samples acquired at 40 and depicted as MW-900-40, MW-1000-40, and MW-1100-40 showed the initial reversible discharge capacities of 506, 360, and 526 mAh/g with the initial Coulombic efficiency 45%, 43%, and 54% correspondingly. Comparing the discharge-charge capacity and coulombic efficiency, the sample acquired at 1100-50 shows significantly better performance among all with higher Coulombic efficiency and discharge capacity (Table S2).

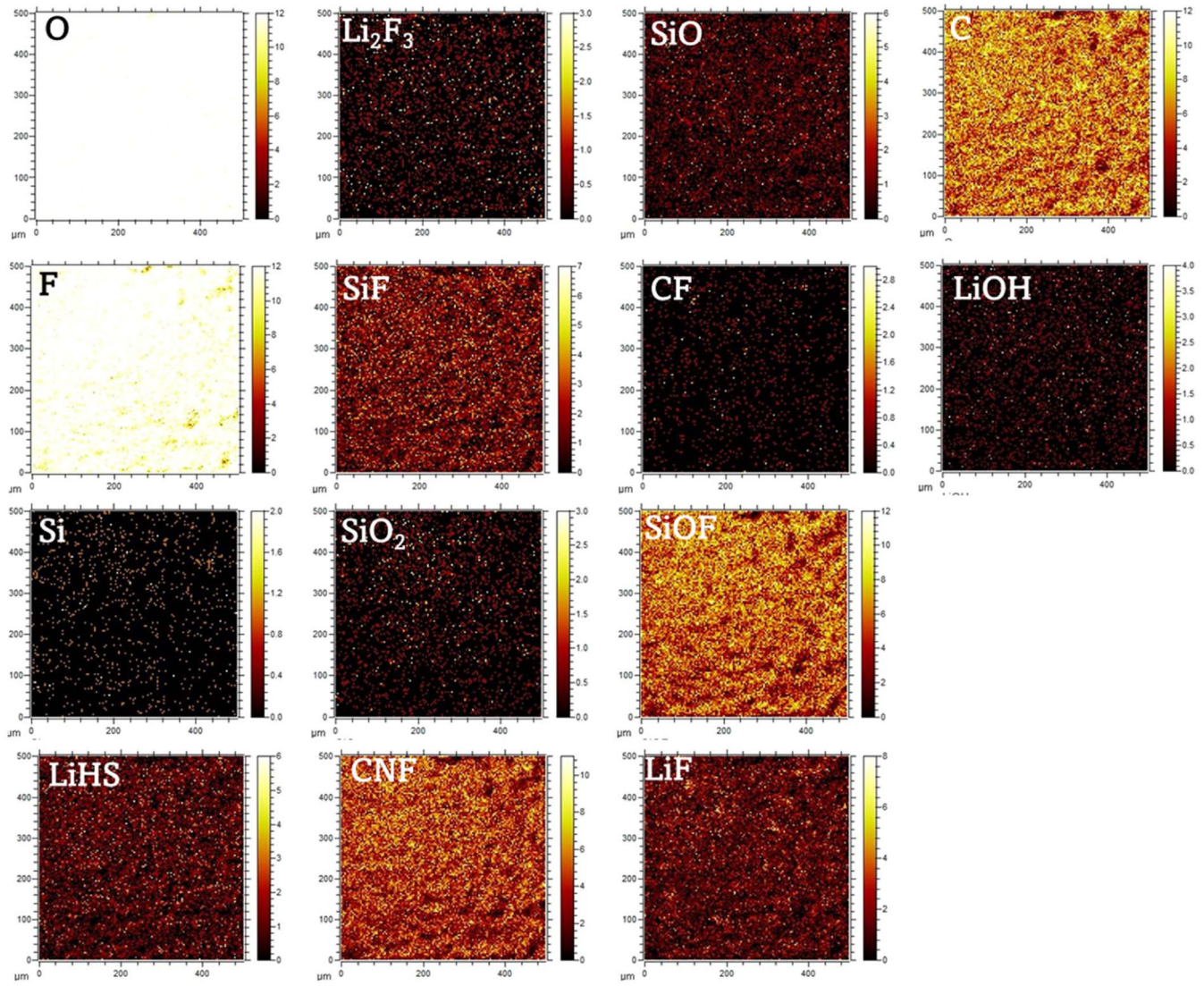

FIGURE 11 ToF-SIMS imaging analysis in negative ion mode of MW-1100-50 electrode delithiated in $LiPF_6$ for LIB at 0.1C current density at 3 V.

Next, we examined the rate performance and cyclic stability of LIBs with all the anode materials acquired via microwave irradiation carbonization process. Figures 7A,B and S10a,d show the dependence of the rate performance on the applied current density starting from 0.1 to 2C. While increasing the current density, the performance showed much less significant difference in all the samples. Subsequently, the MW-1100-50 showed an increase in capacity after returning to a lower current density, thereby accrediting to the better structural stability of the nanocomposite. In other words, the structure containing sustainable composition of partially graphitized carbon along with silicon and silicon carbide as per the XPS and XRD data analysis helps to minimize the volumetric changes of the Si nanocrystals as the crystalline carbon plays the encapsulation layer for the nanocrystal. The electrode MW-1100-50 materials exhibited excellent long-term cycling stability over 120 cycles, retaining ~71% initial capacity of the initial reversible capacities along with ~97% Coulombic efficiency during the entire cycle measurements. Comparing the measurements, MW-900-50 and MW-1000-50 showed exceptional ~94% and ~95% Coulombic efficiency during the entire cycle and cyclic stability.

3.4 | Ex situ study of electrode

To further gain a better understanding of the surface modification of the electrode after initial discharge, discharge-charge in LiPF6 electrolyte was studied only in the case of MW-1100-50 considering the performance.

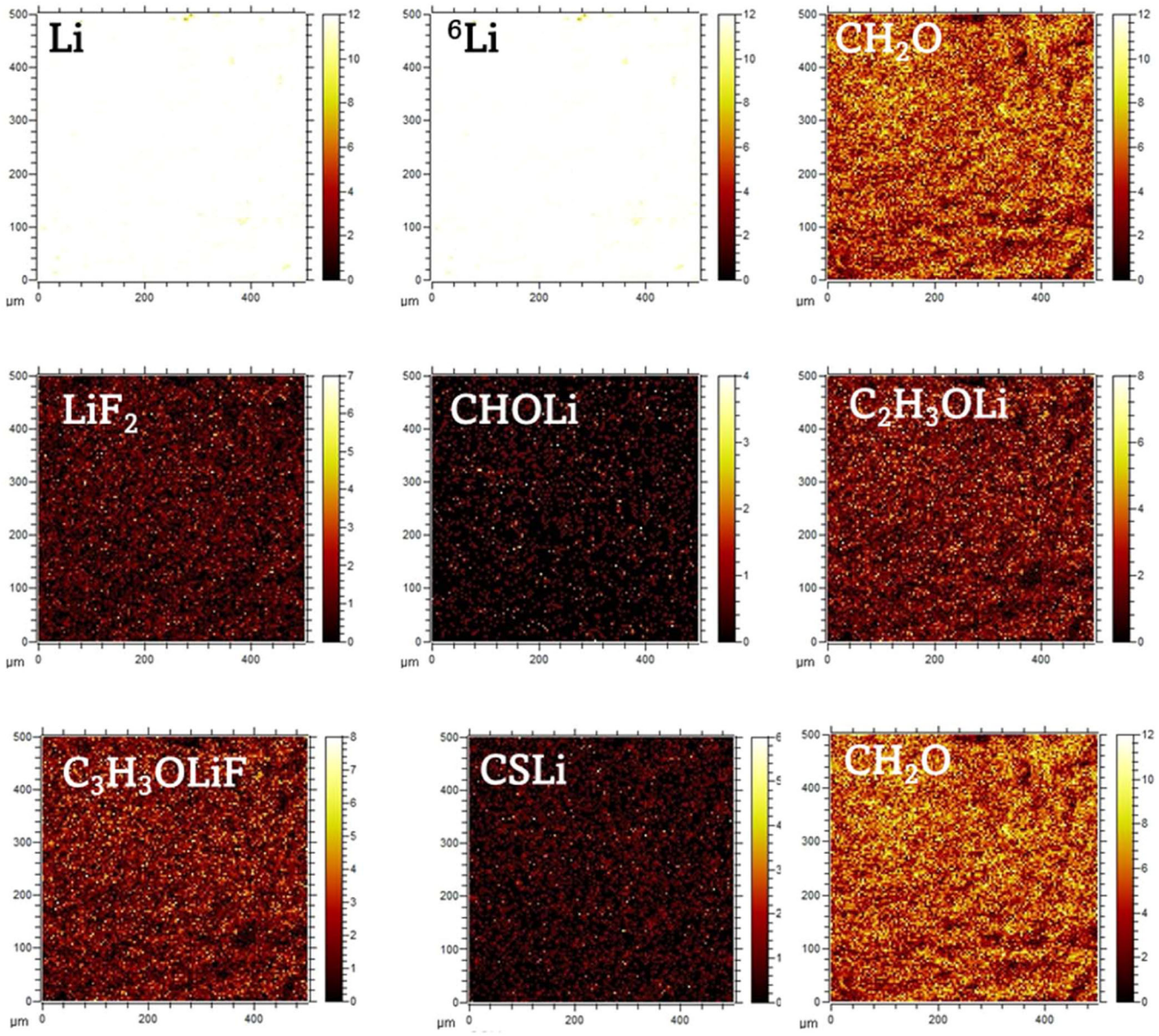

FIGURE 12 ToF-SIMS imaging analysis in positive ion mode of MW-1100-50 electrode delithiated in $LiPF_6$ for LIB at 0.1C current density at 3 V.

The surface morphology was understood by FE-SEM (Figure S11), where the pristine electrode shows a loosely packed, homogenous distribution of carbon and silicon. The fully lithiated electrode shows thick layering with less visible particles seen, which possibly occurred after solid electrode interphase (SEI) formation, thereby covering the entire surface. Upon delithiation, the entire surface seems to have no significant cracking of a surface, and the particle appears independent. The high-resolution spectrum analysis of F1s, O1s, and C1s was performed to understand the composition of the electrode surface. The XPS and ToF-SIMS analysis was performed and results were displayed by spectra plot (Figure 8) imaging (Figures 7–12) and sputter plot (Figure 13A,D). The spectra shows significant presence of various derivatives of fluorinates, carboxylates, oxalates, and peaks of silicon and lithium. In XPS survey, F1s high resolution peak, shows LiF is located at 685 eV, along with $LiPF_6$ at 687 eV followed by the CF at 683 eV as reported earlier in silicon electrode study[24–26] in both delithiated and lithiated sample which concludes that the $LiPF_6$ forms an integral part of the SEI following the dissociation of PF_6 ions into the surface forming LiF a critical component of SEI at the initial cycle.[27] This significantly agrees with the ToF-SIMS data, where LiF, $(CH_2OCO_2Li)_2$, CF, SiOF, and LiF derivatives are observed in both positive and negative ion modes, respectively. These inorganic components mainly

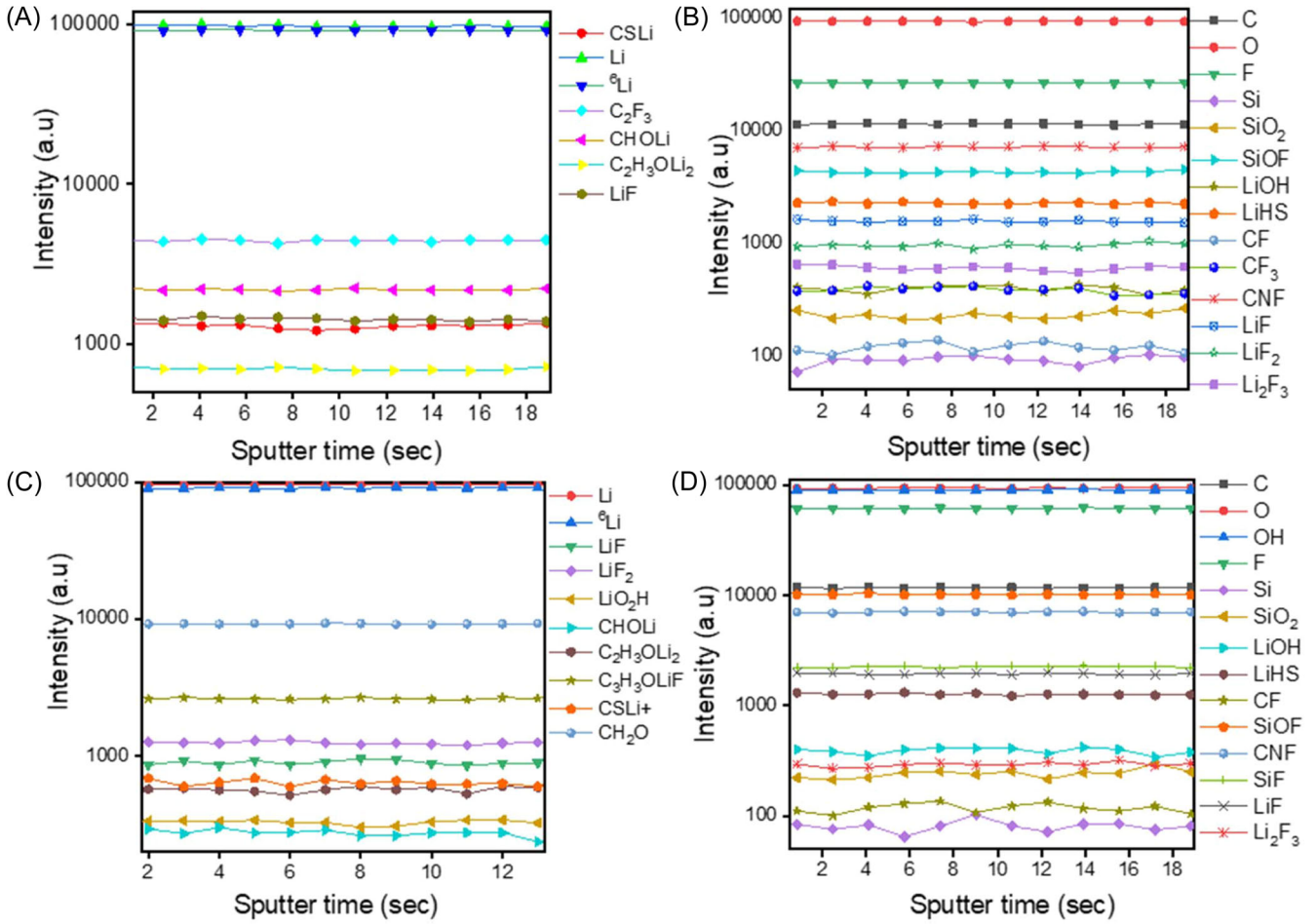

FIGURE 13 ToF-SIMS, sputter plot analysis in (B–D) negative and (A–C) positive ion mode of MW-1100-50 material lithiated (0.01V) and delithiated (3V) electrode in $LiPF_6$ for LIB at 0.1C.

contribute to the outer SEI layer. The O1s spectrum shows oxygenated species formed on the surface of the particles as well as in the SEI layer. The formation of C=O and C-O bonds within ROCO group at ~532 and 533 eV mainly describes the carboxylates.[28] The strong spectrum at ~530 eV also shows the presence of Li_2O, which is formed during the first discharge cycle, consequently decreasing upon additional cycling. The XPS spectrum of C1s peak ranging from 280 to 290 eV,explains the formation of a wide range of carbonate group from electrolyte C-C, C-O_x, C-H, hence forming the carbon network on the surface of cycled electrode. The ToF-SIMS data provide confirmation of the carbonate species on the surface, as observed in the sputter plot and imaging, and the sputtering time and signal intensity of elements F and C can be utilized to gauge the interfacial layer's strength, with the consistency of the element's signal increasing as the sputtering time increases, indicating that the SEI is primarily composed of an inorganic phase from the surface to the inner layer.[29]

4 | CONCLUSION

In this study, we developed a one-step pyrolysis/reduction technique based on microwave irradiation heating using microwave irradiation. The technique is novel and unique to convert the biomass to battery material and further fabricate a composite material consisting of high-purity silicon and highly graphitized carbon (Si@GC) using rice husk as the source material. Unlike conventional heating methods, Si@GC samples were synthesized within a relatively short duration of time (30–50 min) readily reducing the CO_2 emission indirectly through electricity usage. The utilization of ultrahigh heating rates facilitated the successful synthesis of the highly graphitized carbon and crystalline silicon composite. The microwave irradiation process resulted in the production of a homogeneous material with excellent surface area, essential functional groups, and a high degree of crystallinity, thereby demonstrating the exceptional reaction kinetics involved in the material

formation. The as-synthesized Si@GC composite anode material exhibited a remarkable discharge capacity of 799 mAh/g, along with a high cyclic stability of approximately 71% over 120 cycles. The ex situ ToF-SIMS analysis revealed the presence of a notable inorganic SEI composition, primarily consisting of fluorinated species and carbonate species that were generated during the initial cycle. This study describes an innovative and efficient heating process to produce battery materials, which may also be used for a variety of other materials and applications. We anticipate that this method will eventually be adopted by the industry, having a significant impact in these areas.

ACKNOWLEDGMENTS

C. P. is thankful to QUT for the QUTPRA scholarship for doctoral research. The authors acknowledge the facilities and the scientific and technical assistance of staff at the Central Analytical Research Facility (CARF), QUT. D. P. D. acknowledges QUT's start-up grant: 323000-0424/07. H. D. P. and D. P. D. acknowledge the postdoc fellowship sponsored by the Centre for Materials Science and the research support by the Centre for Waste Free World, QUT, Australia.

CONFLICT OF INTEREST

The authors declare no conflict of interest.

DATA AVAILABILITY STATEMENT

The data that support the findings of this study are available from the corresponding author upon reasonable request.

ORCID

Deepak Dubal http://orcid.org/0000-0002-2337-676X

REFERENCES

1. Heidari M, Dutta A, Acharya B, Mahmud S. A review of the current knowledge and challenges of hydrothermal carbonization for biomass conversion. *J Energy Inst*. 2019;92(6):1779-1799.
2. Hu X, Gholizadeh M. Biomass pyrolysis: a review of the process development and challenges from initial researches up to the commercialisation stage. *J Energy Chem*. 2019;39:109-143.
3. Bridgwater AV. Review of fast pyrolysis of biomass and product upgrading. *Biomass Bioenergy*. 2012;38:68-94.
4. Balat M, Balat M, Kırtay E, Balat H. Main routes for the thermo-conversion of biomass into fuels and chemicals. Part 1: pyrolysis systems. *Energy Convers Manage*. 2009;50(12):3147-3157.
5. Adam D. Out of the kitchen. *Nature*. 2003;421(6923):571-572.
6. Gabriel C, Gabriel S, H. Grant E, H. Grant E, S. J. Halstead B, Michael P. Mingos D. Dielectric parameters relevant to microwave dielectric heating. *Chem Soc Rev*. 1998;27(3):213.
7. Zhu Y-J, Chen F. Microwave-assisted preparation of inorganic nanostructures in liquid phase. *Chem Rev*. 2014;114(12):6462-6555.
8. Wang X, Pham HD, Padwal C, et al. Rapid and low-carbon emission synthesis of stable $LiNi_{0.5}Mn_{1.5}O_4$ cathode for Li-Ion batteries. *Adv Energy Sustainability Res*. 2023;5:2300199.
9. Praneetha S, Murugan AV. Development of sustainable rapid microwave assisted process for extracting nanoporous Si from earth abundant agricultural residues and their carbon-based nanohybrids for lithium energy storage. *ACS Sustain Chem Eng*. 2015;3(2):224.
10. Jung DS, Ryou M-H, Sung YJ, Park SB, Choi JW. Recycling rice husks for high-capacity lithium battery anodes. *Proc Natl Acad Sci*. 2013;110(30):12229-12234.
11. Li Y, Liu L, Liu X, et al. Core–shell structured C/SiO_2 composites derived from Si-rich biomass as anode materials for lithium-ion batteries. *Ionics*. 2022;28:1.
12. Cui X, Liu L, Liu X, et al. Carbon-coated rice husk-derived SiO_2/C composites as anodes for lithium-ion batteries: comparison between CTEP and PVC carbon coatings. *J Electron Mater*. 2022;51:68-76.
13. Song J, Guo S, Kou L, et al. Nitrogen-doped carbon/SiO_x composites from rice husks as a high-performance anode for lithium-ion batteries. *J Mater Sci: Mater Electron*. 2020;31:16037.
14. Choi M, Kim J-C, Kim D-W. Waste windshield-derived silicon/carbon nanocomposites as high-performance lithium-ion battery anodes. *Sci Rep*. 2018;8(1):960.
15. Padwal C, Pham HD, Hoang LTM, Mundree S, Dubal D. Deep eutectic solvents assisted biomass pre-treatment to derive sustainable anode materials for lithium-ion batteries. *Sustain Mater Technol*. 2023;35:e00547.
16. Ahmed F, Almutairi G, Hasan PMZ, et al. Fabrication of a biomass-derived activated carbon-based anode for high-performance li-ion batteries. *Micromachines*. 2023;14(1):192.
17. Attolini G, Rossi F, Fabbri F, Bosi M, Salviati G, Watts BE. *Nanowires*. IntechOpen; 2010.
18. Zhu M, Yang Y, Ma Y. Salt assisted synthesis of advanced carbon-based materials for energy related applications. *Green Chem*. 2023;25:10263-10303.
19. Patrick JW. Porosity in Carbons: *Characterization and Applications*. Edward Arnold, CiNii Books; 1995.
20. Sharma I, Deshan ADK, Pham HD, Padwal C, Doherty WOS, Dubal D. Zero-waste: carbon and SiO_2 composite materials from the solid residue of the hydrothermal liquefaction of anaerobic digestion digestate for Li-ion batteries. *Sustain Mater Technol*. 2022;31:e00364.
21. Chu H, Wu Q, Huang J. Rice husk derived silicon/carbon and silica/carbon nanocomposites as anodic materials for lithium-ion batteries. *Colloids Surf A*. 2018;558:495-503.
22. Zhang Y-C, You Y, Xin S, et al. Rice husk-derived hierarchical silicon/nitrogen-doped carbon/carbon nanotube spheres as low-cost and high-capacity anodes for lithium-ion batteries. *Nano Energy*. 2016;25:120-127.
23. Yin Y-X, Xin S, Wan L-J, Li C-J, Guo Y-G. Electrospray synthesis of silicon/carbon nanoporous microspheres as improved anode materials for lithium-ion batteries. *J Phys Chem C*. 2011;115(29):14148-14154.
24. Xu C, Lindgren F, Philippe B, et al. Improved performance of the silicon anode for Li-ion batteries: understanding the

surface modification mechanism of fluoroethylene carbonate as an effective electrolyte additive. *Chem Mater*. 2015;27(7):2591-2599.

25. Philippe B, Dedryvère R, Gorgoi M, Rensmo H, Gonbeau D, Edström K. Role of the $LiPF_6$ salt for the long-term stability of silicon electrodes in Li-ion batterie—a photoelectron spectroscopy study. *Chem Mater*. 2013;25(3):394-404.
26. Lu M, Cagnetta G, Zhang K, Huang J, Yu G. Mechanochemical mineralization of "very persistent" fluorocarbon surfactants–6:2 fluorotelomer sulfonate (6:2FTS) as an example. *Sci Rep*. 2017;7(1):17180.
27. Lee YM, Lee JY, Shim H-T, Lee JK, Park J-K. SEI layer formation on amorphous Si thin electrode during precycling. *J Electrochem Soc*. 2007;154(6):A515.
28. Schroder KW, Celio H, Webb LJ, Stevenson KJ. Examining solid electrolyte interphase formation on crystalline silicon electrodes: influence of electrochemical preparation and ambient exposure conditions. *J Phys Chem C*. 2012;116(37):19737-19747.
29. Wu Z-Y, Deng L, Li J-T, et al. Solid electrolyte interphase layer formation on the Si-based electrodes with and without binder studied by XPS and ToF-SIMS analysis. *Batteries*. 2022;8(12):271.

SUPPORTING INFORMATION

Additional supporting information can be found online in the Supporting Information section at the end of this article.

How to cite this article: Padwal C, Wang X, Pham HD, Hoang LTM, Mundree S, Dubal D. Efficient and swift heating technique for crafting highly graphitized carbon and crystalline silicon (Si@GC) composite anodes for lithium-ion batteries. *Battery Energy*. 2024;3:20240025. doi:10.1002/bte2.20240025